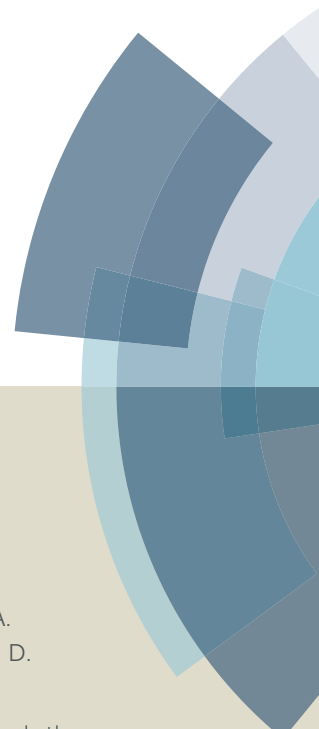
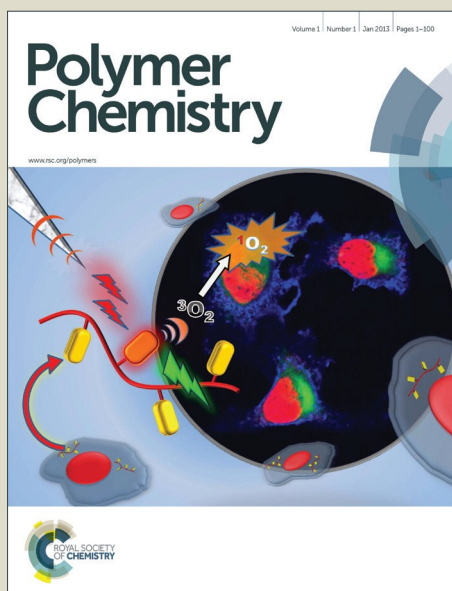


# Polymer Chemistry

Accepted Manuscript



This article can be cited before page numbers have been issued, to do this please use: M. L. Keshtov, A. R. Khokhlov, S.A. Kuklin, I.E. Ostapov, A. Y. Nikolaev, I.O Konstantinov, A. Sharma, E. N. Koukaras and G. D. Sharma, *Polym. Chem.*, 2016, DOI: 10.1039/C6PY01173J.



This is an *Accepted Manuscript*, which has been through the Royal Society of Chemistry peer review process and has been accepted for publication.

*Accepted Manuscripts* are published online shortly after acceptance, before technical editing, formatting and proof reading. Using this free service, authors can make their results available to the community, in citable form, before we publish the edited article. We will replace this *Accepted Manuscript* with the edited and formatted *Advance Article* as soon as it is available.

You can find more information about *Accepted Manuscripts* in the [Information for Authors](#).

Please note that technical editing may introduce minor changes to the text and/or graphics, which may alter content. The journal's standard [Terms & Conditions](#) and the [Ethical guidelines](#) still apply. In no event shall the Royal Society of Chemistry be held responsible for any errors or omissions in this *Accepted Manuscript* or any consequences arising from the use of any information it contains.

## Synthesis and photophysical properties of regioregular low bandgap copolymers with controlled 5-fluorobenzotriazole orientation for photovoltaic application

M. L. Keshtov<sup>a\*</sup>, A. R. Khokhlov<sup>a,b</sup>, S. A. Kuklin<sup>a</sup>, I. E. Ostapov<sup>a,b</sup>, A. Yu. Nikolaev<sup>a</sup>, I. O. Konstantinov<sup>a</sup>, Abhishek Sharma<sup>c</sup>, E. N. Koukaras<sup>d,e</sup>, Ganesh D. Sharma<sup>c\*</sup>

<sup>a</sup>Institute of Organoelement Compounds of the Russian Academy of Sciences, Vavilova St., 28, 119991 Moscow, Russian Federation

<sup>b</sup>Lomonosov Moscow State University, Faculty of Physics, 1-2 Leninskiye Gory, Moscow 119991, Russian Federation

<sup>c</sup>Department of Physics, The LNM of Information Technology (Deemed University), Jamdoli, Jaipur

<sup>d</sup>Nanotechnology and Advanced Materials Laboratory, Department of Chemical Engineering, University of Patras, Patras, 26500 GR, Greece

<sup>e</sup>Molecular Engineering Laboratory, Department of Physics, University of Patras, Patras, 26500 GR, Greece

Two copolymers **P1** and **P2** with regioregular and random structures, respectively, were synthesized and their optical and electrochemical properties (both theoretical and experimental) were investigated. The regioregular copolymer **P1** showed lower optical bandgap and high degree of crystallinity compared to the random **P2** copolymer. These copolymers were used as electron donors along with PC<sub>71</sub>BM as electron acceptor for the fabrication of solution processed bulk heterojunction solar cells. After the optimization of weight ratio between donor and acceptor and the concentration of the solvent additive i.e. DIO in chloroform, the solar cells based on regioregular **P1** exhibit higher power conversion efficiency (7.66 %) than the random **P2** (5.33 %). The enhancement in the power conversion efficiency has been attributed to the increased hole mobility due to high regioregularity of the conjugated copolymer backbone and effective ordering between the polymer chains. This work brings forth and establishes the importance for copolymers to have a regioregular A-D-A-D structure so as to offer significant performance benefits over random D-A copolymer. This approach is a promising new route to materials for highly efficient polymer solar cells.

**Key words:** Regioregular and random D-A copolymers, Bulk heterojunction solar cells, Power conversion efficiency, Solvent additive

\*Corresponding authors

## Introduction

Throughout the last decade, polymer solar cells (PSC) with bulk heterojunction (BHJ) based on nano-composites (polymer donor: fullerene acceptor) have attracted significant attention as renewable energy sources due to their unique advantages, such as low cost, manufacturability, easy possibility for large-area flexible devices manufacturing [1-2], reaching, at same time, impressive progress in PSC effectiveness by more than 10% [3-6]. This progress has been achieved not only through better understanding and control of charge generation and transport, but also via development of a wide range of new narrow bandgap D-A conjugated copolymers [7-8] using generally donor-acceptor (D-A) approach, i.e. copolymers based on alternating fragments of electron donor (D) and electron acceptor (A) units. However, common D-A copolymers have several disadvantages including common polycondensation doesn't permit obtaining regioselective polymers D-A using asymmetrical monomers. It is well known, that electronic and optical properties of D-A copolymers are strongly dependent on structural order. PSC based on regioregular poly(3-hexylthiophene) (P3HT) with alternating regular structures exhibit higher efficiency with light absorption and charge carriers mobility improved by intermolecular  $\pi$ -stacking interactions in comparison with statistical P3HT where substituents are oriented randomly along backbone chain [9]. Moreover the regioregular D-A copolymer showed higher charge carrier mobility that its random counterpart. Recently, Lee et al. synthesized regioregular PBDTTT-C-T copolymer which exhibited narrower optical bandgap (1.55eV) and higher crystallinity degree compared to random polymer PBDTTT-C-T. Inverted PSC based on regioregular PBDTTT-C-T possessed conversion efficiency of 7.79%, which was 19% higher than for PSC based on random PBDTTT-C-T polymer [10]. Müllen and co-workers have also developed random copolymer BFR1 and the corresponding regioregular BFS3 conjugated copolymer. The random BFR1 copolymer had efficiency of 3.91% and the corresponding regioregular BFS3 polymer analogue (as a part of polymer solar cell) was found to have effectiveness of 5.92%, which was 51% higher than that of the PSC based on the random BFR1 copolymer [11]. Using molecular modeling and 2D-GISAXS methods, they have proved conclusively that intermolecular  $\pi$ -stacking interactions have been improved. These data were confirmed by AFM. Thus, photo-absorption improvement and charge carrier mobility increase due to high regioregularity of the conjugated polymers and efficient ordering of polymer chains are the most likely reasons for the increased PSC energy conversion efficiency.

Moreover, fluorination has attracted much attention due to its multiple effects on the optical and electronic properties of resulting copolymers, i.e. the strong withdrawing ability of fluorine atom can effectively modulate the energy levels of copolymers with minor effect on their bandgap and induce the strong dipole along C-F bond resulting in the strong inter/intramolecular interaction which benefits the excitons dissociation and charge transport [12]. Recently, Li et al. have developed a D-A structured copolymer denoted as PBDD-4ff4T with benzodithiophene-4,8-dione acceptor and difluorinated bithiophene (ff2T) as donor unit, used it as donor along with PC<sub>71</sub>BM as acceptor for BHJ PSC and achieved an impressive PCE of 9.2 % without any extra treatment [13].

Inspired by these results, in this article we have synthesized regioregular copolymer **P1** based on fluorine-containing 2,6-bis(7-bromo-6-fluoro-2-hexyl-2*H*-benzotriazol-4-yl)-4,4-bis(2-ethylhexyl)-4*H*-silolo[3,2-*b*:4,5-*b'*]dithiophene (**M3**) and distannyl monomer **M1** and corresponding random D-A polymer analogue **P2** based on asymmetric dibromide 2-hexyl-4,7-dibromo-5-fluorobenzo-1,2,3-triazole (**M2**). As shown in Scheme 2, we present step-by-step synthetic strategy based on A-D-A intermediate, which allows obtaining regioregular polymers through fixed orientation of acceptor unit. To demonstrate this strategy we have chosen monofluorinated precursor, 2-hexyl-4,7-dibromo-5-fluorobenzo-1,2,3-triazole (**M2**), which exhibits asymmetrical reactivity between *ortho*- and *meta*-positions. The obtained random polymer based on **P2** inherently possesses structural disadvantage negatively affecting photovoltaic solar cells characteristics. Due to the fact that acceptor monomer **M2** has an asymmetric molecular structure, it is impossible to control 2-hexyl-5-fluorobenzo-1,2,3-triazole unit orientation in conjugated polymer chain during polycondensation reaction. So, **P2** copolymer generally has random structural regioregularity. Regioregular **P1** exhibits narrow bandgap ( $E_g^{opt} = 1.75$  eV), and higher crystallinity degree compared with random **P2**. These copolymers were used as donor along with PC<sub>71</sub>BM as acceptor for the fabrication of conventional BHJ PSC solar cells. After the optimization of weight ratio of donor to acceptor and concentration of solvent additive (DIO), the PSC based regioregular **P1** showed overall PCE of 7.66 % which is higher than that for random copolymer **P2** (5.33 %) fabricated and characterized under identical conditions.

### Experimental details

The syntheses of starting compounds as well as intermediate monomers are given in the supplementary information.

### Synthesis of copolymers P1

The polymerization was performed by a Stille coupling reaction. In a 50 mL flask, monomers **M1** (0.3722 g, 0.5 mmol) and **M3** (0.5076 g, 0.5 mmol) were dissolved in 15 mL toluene, and the solution was flushed with argon for 15 min, then 27 mg of Pd(PPh<sub>3</sub>)<sub>4</sub> was added into the solution. The mixture was again flushed with argon for 20 min. The reaction mixture was heated to reflux for 48 h. The reaction mixture was cooled to room temperature and added dropwise to 400 mL methanol. The precipitate was collected and further purified by Soxhlet extraction with methanol, hexane, and chloroform in sequence. The chloroform fraction was concentrated and added drop-wise into methanol. Finally, the precipitates were collected and dried under vacuum overnight to get polymer **P1** as a black solid (0.50g, yield 79%). <sup>1</sup>H NMR (CDCl<sub>3</sub>, 400 MHz): δ (ppm) 8.50 - 7.00 (br, 6H, ArH), 4.85(4H, CH<sub>2</sub>-N), 2.27-2.21 (br, 8H, CH<sub>2</sub>-Si), 1.70-0.80 (br, 82H, CH<sub>3</sub>,CH<sub>2</sub>). Elem. Anal, for (C<sub>72</sub>H<sub>100</sub> N<sub>6</sub>S<sub>4</sub>Si<sub>2</sub>)<sub>n</sub>. Calc: C, 67.99; H, 7.92; N, 6.60; S, 10.08; F, 2.99. Found: C, 67.59; H, 7.78; N, 6.34; S, 9.79; F, 2.34.

### Synthesis of copolymers P2

Copolymer **P2** was synthesized by following the same procedure for **P1** but using **M2** instead of **M3**. Monomers **M2** (0.1695 g, 0.5 mmol) and **M1** (0.3722g, 0.5 mmol) were used as starting materials in the polymerization. Finally, **P2** was obtained as a black solid (0.27g, yield 85%). <sup>1</sup>H NMR (CDCl<sub>3</sub>, 400 MHz): δ(ppm) 8.50 -7.00 (br, 3H, ArH), 4.85(2H, CH<sub>2</sub>-N), 2.27-2.21 (br, 4H, CH<sub>2</sub>-Si), 1.70-0.80 (br, 41H, CH<sub>3</sub>, CH<sub>2</sub>). Elem. Anal, for (C<sub>36</sub>H<sub>50</sub>FN<sub>3</sub>S<sub>2</sub>Si)<sub>n</sub> Calc: C, 67.99; H, 7.92; N, 6.60; S, 10.08; F, 2.99, Found: C, 67.65; H, 7.79; N, 6.32; S, 9.71; F,2.64.

### Device fabrication and characterization

BHJ polymer solar cells with conventional structure ITO /PEDOT:PSS / copolymer:PC<sub>71</sub>BM/PFN/Al were prepared on indium tin oxide (ITO) coated glass substrate as follow: An ITO coated glass substrate was cleaned by ultrasonic treatment in deionized water, acetone and isopropyl alcohol sequentially and then dried using nitrogen gas. After that, a thin layer (35 nm) of PEDOT:PSS (poly(3,4-ethylene dioxythiophene): poly(styrenesulfonate)) was spin coated at 3500 rpm for 40 s on the ITO coated glass substrate and subsequently baked at 120

°C for 15 min in air. The copolymers and PC<sub>71</sub>BM (total concentration of 20 mg/ mL) at different weight ratios were dissolved in chloroform and spin coated at 2000 rpm for 1 min on top of the PEDOT:PSS layer. After the optimization of weight ratio of copolymer to PC<sub>71</sub>BM, we have employed solvent additive technique to deposit the active layer film, i.e. copolymer:PC<sub>71</sub>BM (1:2) was dissolved into chloroform with different concentration of DIO and film spin cast described above. The thickness of the active layers was 85-90 nm. Finally a thin layer of aluminium was deposited by thermal evaporation under a shadow mask with a base pressure less than 10<sup>-5</sup> Torr, on top of the active layer. The current–voltage characteristics of the BHJ organic solar cells were measured using a computer controlled Keithley 238 source meter under simulated AM 1.5G, 100 mW/cm<sup>2</sup>. A solar simulator consists with xenon light source coupled with an optical filter was used to provide the stimulated irradiance at the surface of the devices. The incident photon to current efficiency (IPCE) of the devices was measured illuminating the device through the light source and monochromator and the resulting current was measured using a Keithley electrometer under short circuit conditions. The hole-only devices with ITO/PEDOT:PSS/active layer/Au were also fabricated in an analogous way, in order to measure the hole and electron mobilities. All the measurements were performed in the air without an encapsulation of the devices.

## Results and discussion

### Synthesis and characterization

The synthetic routes for the monomers, 2,6-bis(7-bromo-6-fluoro-2-hexyl-2*H*-benzotriazol-4-yl)-4,4-bis(2-ethylhexyl)-4*H*-silolo[3,2-*b*:4,5-*b'*]dithiophene (**M3**) and polymers **P1** and **P2** are shown in Scheme 1. 4,4'-bis(2-ethylhexyl)-5,5'-bis(trimethyltin)-dithieno[3,2-*b*:2',3'-*d*]silole (**M1**) [14], 2-hexyl-4,7-dibromo-5-fluorobenzo-1,2,3-triazole (**M2**) [15] were prepared according to literature methods. As shown in Scheme 1, the palladium catalyzed Stille coupling reaction of the 4,4'-bis(2-ethylhexyl)-5,5'-bis(trimethyltin)-dithieno[3,2-*b*:2',3'-*d*]silole (**M1**) with excess amount (2.5 equivalents) of asymmetric dibromointermediate 2-hexyl-4,7-dibromo-5-fluorobenzo-1,2,3-triazole (**M2**) gave the key monomer, 2,6-bis(7-bromo-6-fluoro-2-hexyl-2*H*-benzotriazol-4-yl)-4,4-bis(2-ethylhexyl)-4*H*-silolo[3,2-*b*:4,5-*b'*]dithiophene (**M3**) in 51% yield. All compounds were purified by silica gel column chromatography, and their structures and purity were fully characterized by multinuclear NMR (<sup>1</sup>H, <sup>13</sup>C and <sup>19</sup>F) spectroscopy (Figure 1), high-resolution mass spectroscopy, and elemental analysis.

Both **P1** and **P2** were synthesized by Stille cross-coupling reaction of dibromide **M2** or **M3** and 4,4'-bis(2-ethylhexyl)-5,5'-bis(trimethyltin)-dithieno[3,2-b:2',3'-d]silole (**M1**) in toluene at 110°C using Pd(PPh<sub>3</sub>)<sub>4</sub> as a catalyst in ~80% yield (Scheme 2). Both polymers were purified by extraction with methanol, acetone and hexane to remove small-molecular weight fractions and catalyst residue. Then the solids were collected by using chloroform as the extraction solvent followed by precipitation in methanol and filtration. The molecular weights ( $M_n$ ) of **P1** and **P2** were determined by GPC with polystyrene as a standard. Regioregular **P1** has average molecular weight ( $M_n$ ) of 20.8 kDa with polydispersity (PDI) of 2.01 while the random polymer **P2** has ( $M_n$ ) of 28.1 kDa with PDI value of 2.08 respectively. Both polymers have similar molecular weights thereby minimizing the influence of molecular weight. Additionally, structures of the two polymers were characterized by elemental analysis and <sup>1</sup>H NMR and <sup>19</sup>NMR. From <sup>1</sup>H NMR spectra (Figure 2) all peaks are broad with respect to the corresponding monomers due to polymeric character. For all polymers, the aromatic protons are observed between 8.50 and 7.00 ppm, the signal of methylene groups adjacent to nitrogen atom appeared around 4.85 ppm. There is a peak at  $\delta$  2.27-2.21 ppm which is attributed to methylene groups directly linked to a silicon atom. The peaks in the ranges of  $\delta$  1.70-0.80 ppm related to other hydrogen protons of the alkyl groups of polymers. In the <sup>1</sup>H NMR spectrum of **M3** the singlet peak at 8.11 ppm should be assigned for proton of the dithienosilole unit while the doublet signal at 7.42-7.54 ppm due to F-benzotriazole unit (it is split into doublet due to spin-coupling with F substituent). It might be proved additionally by comparison of <sup>1</sup>H NMR spectrum of **M2**, which has a doublet signal in the same region, which related to proton at the next position to F-atom (see the Supporting Information, Fig. S1). Indeed, the dithienosilole monomer **M1** has the singlet signal in the region of 7 ppm (7.13 ppm, see Supporting information, Fig. S2), but we believe that in the case of **M3** it has an electron-withdrawing groups such as BTA and the corresponding signal moves into low-field region. The <sup>13</sup>C NMR of **M2** and **M3** is shown in Figure S5 (supporting information) also confirm the chemical structure of these monomers. Taking into account these considerations, we can conclude, that in the spectrum of polymer **P1** (and **P2**) the signals in the region of 8.0-8.5 ppm due to dithienosilole unit and signals in the region of 7.5 ppm correspond to F-BTA unit. All of the integral ratios of peak areas between the aromatic and aliphatic signals agree with corresponding molecular structure of the polymers.

Indeed,  $^1\text{H}$  NMR spectra of the polymers **P1** and **P2** are very similar. But it is obviously because they are built from COMPLETELY identical building blocks. We can conclude, that this type of regioregularity (or non-regularity) of the polymers does not affect their NMR spectra (at least in this case). The spectrum of **P1** (and **P2**) shows two signals of DTS-fragments (at 8.1 and 8.2 ppm). It is believed that they are related to two different fragments of DTS, differently positioned with respect to fluorine atoms. The complex structure of the signal of F-BTA moiety (in the range of 7.43 ppm) can be explained by S...F contacts between DTS and BTA fragments. These contacts can partially prevent the internal rotation of the structural units and additionally contribute to macromolecular order of the polymer chains in the bulk. We can suggest that some of these possible contacts are not realized so structurally non-equivalent H-atoms of the BTA-fragments can appear, which make the NMR spectra more complex.

The thermal properties of **P1** and **P2** were evaluated by differential scanning calorimetry (DSC) and thermogravimetric analysis (TGA) measurements. TGA curves for **P1** and **P2** are shown in Figure 3. **P1** and **P2** exhibit good thermal stability with 5% weight-loss temperature ( $T_d$ ) at 350°C and 381° C, respectively under  $\text{N}_2$ . They were thermally stable for applications in optoelectronic devices. The DSC curves of **P1** and **P2** displayed no phase transition in the range 25-300°C.

### Optical and Electrochemical Properties

The UV-visible absorption spectra of the **P1** and **P2** in chloroform solutions and in thin films are shown in Figure 4 and corresponding optical data are summarized in Table 1. Both polymers showed a strong absorption peak around 600 nm (molar extinction coefficient  $3.4 \times 10^5$  and  $2.45 \times 10^5 \text{ mol}^{-1} \text{ cm}^{-1}$  for **P1** and **P2**, respectively) originating from delocalized excitonic  $\pi$ - $\pi^*$  transitions of conjugated polymer backbone. Interestingly, the regioregular **P1** exhibited stronger absorption intensity than the random **P2** which could be ascribed to vigorous  $\pi$ - $\pi^*$  transitions of conjugated polymer chain. In dilute solutions, the main absorption band of regioregular polymer **P1** is bathochromically shifted by 15 nm and broadened to some extent in comparison to that of its random counterpart **P2**. This difference can be attributed to enhanced intermolecular  $\pi$ - $\pi$  interactions resulting from the regioregular arrangement of the polymer main chain [16]. In the solid-state absorption spectra these differences were even more pronounced. It was found that the absorption spectrum of **P1** in solid thin film has a stronger shoulder peak at 641nm than those of

random **P2**, indicating good intermolecular  $\pi$ - $\pi^*$  stacking of regioregular **P1**. This result clearly indicates that the structural regioregularity of the conjugated backbones in **P1** copolymers can have a significant effect on their optical properties. The maximum absorption peak of **P1** was at 592, and 578 nm for **P2** with an onset absorption wavelengths at 707 nm and 693 nm corresponding to an optical bandgap ( $E_g^{opt}$ ) of 1.75 eV and 1.79 eV, respectively.

The Electrochemical properties of polymers were investigated to elucidate the HOMO and LUMO energy levels. The cyclic voltammetry characteristics of these copolymers are illustrated in Figure 5 and the relevant data are summarized in Table 1. HOMO and LUMO energy levels, electrochemical band gaps ( $E_g^{ele}$ ) are -5.40 eV/-3.40 eV and 2.00 eV for **P1** and -5.31 eV/-3.33 eV and 1.96 eV for **P2**, respectively, according to the following equations of  $E_{HOMO} = -e(E_{ox} + 4.40)$  eV and  $E_{LUMO} = -e(E_{red} + 4.4)$  eV. Deep HOMO energy levels of **P1** and **P2** were desired for achieving a higher  $V_{oc}$  in the PSCs and made these copolymers promising candidates for use as polymer donor materials. The LUMO levels of the polymers are higher than that of LUMO PC<sub>71</sub>BM (-4.1 eV) and the differences between the LUMO levels of the polymers and PC<sub>71</sub>BM are 0.79 eV and 0.86 eV, for **P1** and **P2**, respectively. Consequently, the electron transfer from the polymers (electron donor) to PC<sub>71</sub>BM (electron acceptor), which is the essential process for the charge separation of the excitons, can be allowed [14]. The  $E_g^{ele}$  values of **P1** and **P2** is larger (0.25-0.17 eV) than  $E_g^{opt}$  values. This discrepancy between the electrochemical and optical band gaps presumably resulted from the exciton binding energies of the polymers and/or the energy barrier at the interface between the polymer film and the electrode surface [15].

In order to get information about the molecular stacking of the copolymers, X-ray diffraction patterns were measured for the regioregular **P1** and random **P2** films (Figure 6). The copolymer **P1** and **P2** showed the pronounced diffraction peaks at  $2\theta = 5.28^\circ$  and  $4.64^\circ$ , respectively. These diffraction peaks corresponds to the lamellar  $d_{100}$  spacing which originated from the separation between the conjugated copolymer backbones and depends on the length as well as the orientation of side chains, was estimated to be 16.82 Å and 17.56 Å for regioregular **P1** and random **P2**, respectively. In addition to above, the strong and wider diffraction peaks at  $2\theta = 22.48^\circ$  and  $22.04^\circ$  for **P1** and **P2** films, respectively were observed in XRD pattern, which assigned to  $d_{010}$ -spacing. The  $d_{010}$  spacing corresponds to the  $\pi$ - $\pi$  stacking distance of the

conjugated polymer backbones of 3.64 Å and 3.98 Å in the regioregular **P1** and random **P2**, respectively. Moreover, the intensity of  $d_{010}$  peak in the **P1** is much stronger than that in **P2**. The XRD results clearly indicate that the degree of crystallinity in **P1** is higher than that for **P2**.

### Theoretical Calculations

We have additionally performed a theoretical study on the **P1** and **P2** molecular structures within the framework of density functional theory (DFT) and time-dependent density functional theory (TD-DFT).

The initial geometry optimization calculations were performed employing the gradient corrected functional PBE [17] of Perdew, Burke and Ernzerhof. The def-SVP basis set [18] was used for all of the calculations. At this stage of the calculations, to increase the computational efficiency (without loss in accuracy), the resolution of the identity method [19] was used for the treatment of the two-electron integrals. Subsequent geometry optimizations were further performed using the hybrid exchange–correlation functional B3LYP [20] as well as Truhlar’s meta-hybrid exchange–correlation functional M06 [21], and the same basis set. Tight convergence criteria were placed for the SCF energy (up to  $10^{-7}$  Eh) and the one-electron density (rms of the density matrix up to  $10^{-8}$ ) as well as for the norm of the Cartesian gradient (residual forces both average and maximum smaller than  $1.5 \times 10^{-5}$  a.u.) and residual displacements (both average and maximum smaller than  $6 \times 10^{-5}$  a.u.). Solvent effects were included for chloroform (CF) using the integral equation formalism variant of the Polarizable Continuum Model (IEFPCM), as implemented in the Gaussian package [22].

TD-DFT excited state calculations were performed to calculate the optical gaps of **P1** and **P2** using the same functionals and basis set on the corresponding ground state structures. The UV/Vis spectra were calculated using the B3LYP and M06 functionals. The first round of geometry optimizations was performed using the Turbomole package [23]. All of the follow up calculations were performed using the Gaussian package [22].

The first round of calculations was the geometry optimizations of the **P1** and **P2** structures. To increase the computational efficiency, the alkyl groups were truncated to ethyl groups. Vibrational analysis on the optimized structures did not reveal any vibrational modes with imaginary eigenfrequencies, i.e. the final optimized structures are true local (if not global)

minima. The dimmer was considered for the **P2** so that it is properly analogous to the **P1** structure. Both of the structures are nearly perfectly planar (not including the alkanes), in gas phase as well as in solvent. We have calculated the HOMO and LUMO energy levels and the optical gaps, defined here as the energetically lowest allowed vertical electronic excitation, employing the PBE, M06, and B3LYP functionals. In Table 2, in addition to the frontier orbitals' energy levels, we also provide the optical gap the main contributions to the first excitation as well as the wavelength of the first excitation and of the excitations with the largest oscillator strengths.

In addition to the B3LYP functional we have also performed our calculations employing the M06 functional. The M06 meta-hybrid functional was chosen since it provides leveled performance over transition types [24, 25]. We provide results using all three functionals, which can additionally be used for comparison with the literature.

The HOMO–LUMO (HL) gap of each structure calculated using the hybrid B3LYP functional is notably smaller, by  $\sim 0.4$  eV, than that using the meta-hybrid M06 functional, however, the calculated optical gaps are only marginally smaller, with a difference  $\sim 0.1$  eV. In Table 2, we also provide the character of the first allowed excitations only for contributions larger than 4%. The first excitation, as calculated by each of the functional for all three structures, clearly exhibits a single-configuration character.

In Figure 7, we have plotted the isosurfaces (isovalue=0.02) of the HOMO and LUMO for both structures. In both cases the HOMO extends evenly over the main body. For the LUMO of each structure the delocalizations are also similar. The LUMO of **P1** and **P2** extends over the main structure but considerably more over the triazole group than in the case of the respective HOMOs. To quantify the contributions of the moieties to the frontier orbitals we have calculated the total and partial density of states (PDOS). The PDOSs for **P1** and **P2** are shown in Figure S6 (supplementary information). We partition all of the structures into the silolodithiophene (**SDT**) and fluorobenzotriazole (**FBT**) moieties. As expected, structures **P1** and **P2** have significant similarities on the delocalization of the frontier orbitals. The contributions of the **SDT** and **FBT** moieties to the HOMO of **P1** are 71.3% and 28.5%, respectively, and for **P2** at 70.4% and 29.4% respectively. For the LUMO of **P1** the contributions of the **SDT** and **FBT** moieties are 50.0% and 48.4%, respectively, and for **P2** at 50.2% and 48.2%, respectively. We note that, besides their

similarities, structures **P1** and **P2** exhibit different dipole moments which is reflected in difference in their solubility.

In Figure 8, we show the UV/Visual absorption spectra of the **P1** and **P2** structures calculated at the TD-DFT/M06 level of theory, both accounting for solvent effects for CF and in gas phase. The spectra have been produced by convoluting Gaussian functions with HWHM = 0.22 eV centered at the excitation wavenumbers. In Figure S7 (see Supporting Information) we also provide the corresponding spectra calculated using the B3LYP functional, which is in remarkable agreement with the spectra using the M06 functional, and only slightly underestimates in the long wavelength region (by ~40 nm). The calculated absorption spectra of **P1** and **P2** are almost the same and they exhibit one main band with high absorbance, at ~555 nm, as well as a low intensity peak at smaller wavelengths at ~280 nm. The theoretical absorption spectra closely matched with the experimentally observed absorption spectra.

### Photovoltaic properties

In order to examine the influence of the structural regioregularity of conjugated copolymer backbones on the photovoltaic performance of solar cell devices, conventional BHJ polymer solar cells were fabricated with structure of ITO/PEDOT:PSS/copolymer:PC<sub>71</sub>BM/PFN/Al. The active layers were spin coated from copolymer/PC<sub>71</sub>BM solutions prepared from either CF or 1,8-diiiodooctane (DIO, 3v %)-CF mixture. First of all, we have varied the weight ratio of copolymer to PC<sub>71</sub>BM in chloroform solution and found the best photovoltaic response was observed for the active layers with weight ratios of 1:2 for both copolymers and the photovoltaic parameters are compiled in Table 3. Without DIO the devices showed PCE of 3.87 % ( $J_{sc}$  = 8.58 mA/cm<sup>2</sup>,  $V_{oc}$  = 0.98 V and  $FF$  = 0.46) and 2.53 % ( $J_{sc}$  = 6.88 mA/cm<sup>2</sup>,  $V_{oc}$  = 0.92 V and  $FF$  = 0.40) for **P1** and **P2**, respectively. In order to improve the PCE further, we have employed solvent additive method as reported in the literature for PSCs [26]. We are only discussing the results on the devices based on optimized active layer, i.e. weight ratio of copolymer to PC<sub>71</sub>BM is 1:2 and concentration of DIO is 3 v% in CF. The current –voltage ( $J$ - $V$ ) characteristics of devices based on **P1**:PC<sub>71</sub>BM and **P2**:PC<sub>71</sub>BM processed with DIO (3v%)/CF are shown in Figure 9a and photovoltaic parameters are compiled in Table 3. It can be seen from Figure 9a and Table 3 that a clear improvement in PCE was observed in going from random (**P2**) (5.33 %) to regioregular (**P1**)

(7.66 %) copolymer. The higher value of  $V_{oc}$  for **P1** as compared to **P2** is related to the deeper HOMO level of **P1** as compared to **P2**. Moreover, compared to the PSC with random **P2**, the improvement in PCE of the PSC with **P1** may also result from enhanced values of  $J_{sc}$  and FF.

The IPCE spectra of the devices were investigated and shown in Figure 9b. The IPCE spectra of the devices closely resembles with the absorption spectra of the blended active layers. The response in the short wavelength region of 350-500 nm, is attributed to the contribution of PC<sub>71</sub>BM [27]. The IPCE spectra in the longer wavelength region (500 -750 nm) correspond to the absorption of copolymers and are different for these devices. The values of IPCE for the device based on **P1** are higher than that for **P2**, that also supports the higher value of  $J_{sc}$  for the former polymer than for the later one. The integrated values of  $J_{sc}$  from the IPCE spectra are about 12.86 mA/cm<sup>2</sup> and 9.92 mA/cm<sup>2</sup> for **P1** and **P2** based solar cells, respectively, confirming the accuracy of  $J$ - $V$  characteristics of solar cells under illumination.

It is well known that the charge carrier mobility in the active layer is very important in polymer solar cells. In order to get information about the influence of the intermolecular interactions on the hole mobility of the active layers, we have prepared the hole only and electron only devices and measured the hole and electron mobilities in the active layers based on **P1**:PC<sub>71</sub>BM and **P2**:PC<sub>71</sub>BM films. The measured  $J$ - $V$  characteristics of the hole and electron only devices are shown in Figure 10 and charge carrier mobilities are estimated by fitting these curves with space charge limited current model [28]. The hole mobility values for **P1**:PC<sub>71</sub>BM and **P2**:PC<sub>71</sub>BM are  $1.16 \times 10^{-4}$  and  $8.04 \times 10^{-5}$  cm<sup>2</sup>/Vs, respectively. The regioregular **P1** showed an improved mobility compared to random **P2**. This may be attributed to the highly improved  $\pi$ - $\pi$  stacking due to structural regioregularity of conjugated copolymer backbones [29]. This is also supported by the observed red-shift and clear vibronic shoulder in absorption spectrum of **P1** in thin film in the longer wavelength region. Moreover, XRD data also clearly indicate that the improved hole mobility of regioregular **P1** due to high regioregularity of conjugated polymer chains and effective ordering between polymer chains may be the most likely reason for enhancement of PCE [30]. The electron mobilities for **P1**:PC<sub>71</sub>BM and **P2**:PC<sub>71</sub>BM are about  $2.56 \times 10^{-4}$  and  $2.42 \times 10^{-4}$  cm<sup>2</sup>/Vs, respectively. Therefore, the ratios of electron to hole mobilities are 2.19 and 3.00, for **P1**:PC<sub>71</sub>BM and **P2**:PC<sub>71</sub>BM based devices, respectively, indicating more

balanced charge transport in the device based on **P1**:PC<sub>71</sub>BM as compared to **P2**:PC<sub>71</sub>BM, leading to higher value of *FF* and PCE.

The nanoscale morphology of **P1**:PC<sub>71</sub>BM and **P2**:PC<sub>71</sub>BM thin films processed with DIO/CF solvent was investigated using transmission electron microscopy (TEM) and shown in Figure 11. It can be seen from Figure 11 that both the active layers processed with DIO/CF exhibit nanoscale features, indicating fine phase separation of copolymers and PC<sub>71</sub>BM with DIO additive [31]. The black domain is assigned to PC<sub>71</sub>BM aggregation because its ordered aggregation gives relatively high electron density compared to polymer aggregation [32]. The **P1**:PC<sub>71</sub>BM film has more uniform morphology and better interpenetrating networks than **P2**:PC<sub>71</sub>BM film. The **P1**:PC<sub>71</sub>BM layer showed a finer network of bright and dark regions with appropriate nanoscale phase separation between the copolymer **P1** and the PC<sub>71</sub>BM phase, which is beneficial for exciton dissociation and charge transport, resulting in improved *J<sub>sc</sub>*, *FF* and PCE.

In order to get information about the charge generation in the devices based on **P1**:PC<sub>71</sub>BM and **P2**:PC<sub>71</sub>BM due to the different structures of copolymers, we measured the photocurrent density (*J<sub>ph</sub>*) as a function of effective voltage (*V<sub>eff</sub>*) and shown in Figure 12. The measured *J<sub>ph</sub>* is defined as  $J_{ph} = J_L - J_D$ , where *J<sub>L</sub>* and *J<sub>D</sub>* are the current density under illumination (100 mW/cm<sup>2</sup>) and in dark, respectively. *V<sub>eff</sub>* is given as  $V_{eff} = V_o - V_{appl}$ , where *V<sub>o</sub>* is the compensation voltage at which *J<sub>ph</sub>* = 0 and *V<sub>appl</sub>* is the applied voltage. It can be seen from *J<sub>ph</sub>*-*V<sub>eff</sub>* plots that at low *V<sub>eff</sub>*, the *J<sub>ph</sub>* increases linearly with *V<sub>eff</sub>* and tend to saturate at higher *V<sub>eff</sub>* in both the devices, at which the internal electric field is large enough to dissociate all the photogenerated excitons into free charge carriers. This voltage is also responsible to sweep out all free charge carriers towards the electrodes [33]. We have observed that the *J<sub>ph</sub>* starts to saturate at lower *V<sub>eff</sub>* for **P1**:PC<sub>71</sub>BM as compared to **P2**:PC<sub>71</sub>BM, indicating that due to regioregular nature of **P1** with the enhanced intermolecular interactions, the low internal electric field is needed to sweep out the charge carriers in this device as compared to **P2** based device. We have estimated the probability of charge collection (*P<sub>c</sub>*) of separated carriers using  $P_c = J_{sc}/J_{phsat}$  and the values of *P<sub>c</sub>* are 0.86 and 0.80 for **P1**:PC<sub>71</sub>BM and **P2**:PC<sub>71</sub>BM based devices, respectively. The higher value of *P<sub>c</sub>* for the **P1**:PC<sub>71</sub>BM device is attributed to the better nanoscale morphology and balanced charge transport.

We have estimated the series resistance ( $R_s$ ) and shunt resistance ( $R_{sh}$ ) from the slope of the J–V characteristics of the devices, under illumination, around the  $V_{oc}$  and  $J_{sc}$ , respectively, and compiled them in Table 3. In general, the  $R_s$  of the organic solar cell is composed of the bulk resistance of the active layer and depends on the charge transport ability within the active layer and the morphology of the active layer. It can be seen from Table 3 that  $R_s$  of the device based on **P1**:PC<sub>71</sub>BM is lower than that for **P2**:PC<sub>71</sub>BM which may be attributed to better morphology and balanced charge transport. The increase in  $R_{sh}$  is related to the decrease in leakage current and depends upon the intermolecular interaction (or electronic) coupling between the donor and acceptor materials in the active layer.

### Conclusion

Two copolymers **P1** (regioregular) and **P2** (random) were successfully synthesized. Regioregular copolymer **P1** showed slightly lower optical bandgap (1.75 eV) and higher crystallinity compared to random copolymer **P2**. These copolymers were used as donor materials along with PC<sub>71</sub>BM as acceptor for the fabrication of bulk heterojunction PSCs. After the optimization of active layers (weight ratio between copolymers and PC<sub>71</sub>BM and concentration of solvent additive), PSC based on **P1** shows conversion efficiency of 7.66 % which is higher than for the random copolymer **P2** (5.33 %). Improved photo-absorption and charge carriers mobility due to high regioregularity of conjugated copolymers and efficient ordering of copolymer chains are most likely cause of PSC energy conversion efficiency increasing. This study suggests that **P1** copolymer can achieve high PCE due to increase in structural regioregularity of conjugated polymer chains. Although, both the active layers processed with DIO/CF show uniform nanoscale features however the **P1**:PC<sub>71</sub>BM film exhibits more uniform morphology and better interpenetrating networks than **P2**:PC<sub>71</sub>BM film, resulting in improved  $J_{sc}$ ,  $FF$  and PCE. Moreover, the approach we have described here also provides an opportunity to further modulate the optical and electronic properties of conjugated copolymers through the use of two different donor units.

### Acknowledgement

This work is supported by the Russian Science Foundation (grant number 14-13-01444).

## References

1. Gendron, D.; Leclerc, M.; *Energy Environ. Sci.*, **2011**, 4, 1225
2. Dou, L.; You, J.; Yang, J.; Chen, C.-C.; He, Y.; Murase, S. Moriarty, T.; Emery, K.; Li, G.; Yang, Y. *Nat. Photonics*, **2012**, 6,180.
3. Weiwei Li, Alice Furlan, Koen H. Hendriks, Martijn M. Wienk, and René A. J. Janssen J. Am. Chem. Soc. 2013,135, pp 5529–5532
4. Huiqiong Zhou, Yuan Zhang, Cheng-Kang Mai, Samuel D. Collins, Guillermo C. Bazan, Thuc-Quyen Nguyen and Alan J. Heeger, *Adv. Mater.* 2015, 27, 1767-1773
5. T. L. Nguyen, H. Choi, S.-J. Ko, M. A. Uddin, B. Walker, S. Yum, J.-E. Jeong, M. H. Yun, T. J. Shin, S. Hwang, J. Y. Kim and H. Y. Woo *Energy Environ. Sci.*, 2014, 7, 3040-3051
6. (a) Long Ye, Shaoqing Zhang, Wenchao Zhao, Huifeng Yao, and Jianhui Hou , *Chem. Mater.* 2014, 26, 3603–3605, (b) Jingbo Zhao, Yunke Li, Guofang Yang, Kui Jiang, Haoran Lin, Harald Ade, Wei Ma, He Yan, *Nature Energy*, 2016, 1, 15027, (c) Xiaopeng Xu, Zuoqia Li, Zhenguo Wang, Kai Li, Kui Feng, Qiang Peng, *Nano Energy* , 2016, 25, 170-183
7. F. C. Krebs, *Sol. Energy Mater. Sol. Cells*, 2009, 93, 393
8. Y. Li, *Acc. Chem. Res.*, 2012, 45, 723
9. (a) Wu, P. T.; Xin, H.; Kim, F. S.; Ren, G.; Jenekhe, S. A. *Macromolecules*, **2009**, 42, 88, (b) Pascui, O. F.; Lohwasser, R.; Sommer, M.; Thelakkat, M.; Thurn-Albrecht, T.; Saalwachter, K. *Macromolecules*, **2010**, 43,9401, (c ) L. A. Perez, P. Zalar, L. Ying, K. Schmidt, M. F. Toney, T. Q. Nguyen, G. C. Bazan, E. J. Krame, *Macromolecules*, 2014, 47, 1403–1410
10. Honggi Kim, Hyungjin Lee, Donghyun Seo, Youngjun Jeong, Keun Cho, Jaechol Lee, and Youngu Lee, *Chem. Mater.*, DOI: 10.1021/acs.chemmater.5b00632
11. Tianshi Qin, Wojciech Zajaczkowski, Wojciech Pisula, Martin Baumgarten, Ming Chen, Mei Gao, Gerry Wilson, Christopher D. Easton, Klaus Müllen, and Scott E. Watkins, *J. Am. Chem. Soc.* 2014, 136, 6049–6055
12. (a) W. Li, S. Albrecht, L. Yang, S. Roland, J. R. Tumbleston, T. McAfee, L. Yan, M. A. Kelly, H. Ade, D. Neher, W. You, *J. Am. Chem. Soc.* **2014**, 136, 15566, (b) D. Dang, W. Chen, S. Himmelberger, Q. Tao, A. Lundin, R. Yang, W. Zhu, A. Salleo, C. Müller, E. Wang, *Adv. Energy Mater.* **2014**, 4, 1400680, (c) Q. P. Fan, Y. Liu, H. Jiang, W. Su, L. Duan, H. Tan, Y. Li, J. Deng, R. Yang, W. G. Zhu, *Org. Electron.* **2016**, 33, 128, (d) P. Liu, K. Zhang, F. Liu, Y. Jin, S. Liu, T. P. Russell, H. Yip, F. Huang, Y. Cao, *Chem. Mater.* **2014**, 26, 3009, (e) J. Jheng, Y. Lai, J. Wu, Y. Chao, C. Wang, C. Hsu, *Adv. Mater.* **2013**, 25, 2445, (f) J. W. Jung, F. Liu, T. P. Russell, W. H. Jo, *Adv. Energy Mater.* **2015**, 5,1500065, (f) D. Liu, W. Zhao, S. Zhang, L. Ye, Z. Zheng, Y. Cui, Y. Chen, J. H. Hou, *Macromolecules* **2015**, 48, 5172, (g) S. Q. Zhang, L. Ye, J. H. Hou, *Adv. Energy Mater.*

- 2016, 6, DOI: 10.1002/aenm.201502529, (h) Qiang Peng, Xiangju Liu, Dan Su, Guanwen Fu, Jun Xu, Liming Dai, *Adv. Mater.* **2011**, 23, 4554-4558, (i) Kai Li, Zuoqia Li, Kui Feng, Xiaopeng Xu, Lingyan Wang, and Qiang Peng *J. Am. Chem. Soc.*, **2013**, 135, 13549–13557, (j) Yuchong Yang, Renming Wu, Xin Wang, Xiaopeng Xu, Zuoqia Li, Kai Li and Qiang Peng *Chem. Commun.* **2014**, **50**, 439-441
13. Qunping Fan, Wenyan Su, Xia Guo, Bing Guo, Wanbin Li, Youdi Zhang, Kun Wang, Maojie Zhang, and Yongfang Li, *Adv. Energy Mater.* doi: 10.1002/aenm.201600430
14. J.-L. Bredas, D. Beljonne, V. Coropceanu, J. Cornil, *Chem. Rev.* 104, 4971–5004 (2004), L. Zhang, K. Pei, M. Yu, Y. Huang, H. Zhao, M. Zeng, Y. Wang, J. Gao, *J. Phys. Chem. C* 2012, 116, 26154–26161
15. Y. F. Li, Y. Cao, J. Gao, D. L. Wang, G. Au, A. J. Heeger, *Synth. Met.* 1999, 99, 243
16. (a) Szarko, J. M.; Guo, J. C.; Liang, Y. Y.; Lee, B.; Rolczynski, B. S.; Strzalka, J.; Xu, T.; Loser, S.; Marks, T. J.; Tu, L. P.; Chen, L. X. *Adv. Mater.* 2010, 22, 5468–5472. (b) Yiu, A. T.; Beaujuge, P. M.; Lee, O. P.; Woo, C. H.; Toney, M. F.; Fréchet, J. M. J. *Am. Chem. Soc.* 2012, 134, 2180–2185.
17. Perdew, J. P.; Burke, K.; Ernzerhof, M. *Phys. Rev. Lett.* **1996**, 77, 3865–3868.
18. A. Schafer, H. Horn and R. Ahlrichs, *J. Chem. Phys.* **1992**, 97, 2571.
19. Eichkorn, K.; Treutler, O.; Öhm, H.; Häser, M.; Ahlrichs, R. *Chem. Phys. Lett.* **1995**, 240, 283.
20. (a) Becke, A. D. *J. Chem. Phys.* **1993**, 98, 5648–5652. (b) Lee, C.; Yang, W.; Parr, R. G. *Phys. Rev. B* **1988**, 37, 785–89.
21. Zhao, Y.; Truhlar, D.G. *Theor. Chem. Acc.* **2008**, 120, 215–241.
22. Frisch, M. J.; Trucks, G. W.; Schlegel, H. B.; Scuseria, G. E.; Robb, M. A.; Cheeseman, J. R.; Scalmani, G.; Barone, V.; Mennucci, B.; Petersson, G. A.; Nakatsuji, H.; Caricato, M.; Li, X.; Hratchian, H. P.; Izmaylov, A. F.; Bloino, J.; Zheng, G.; Sonnenberg, J. L.; Hada, M.; Ehara, M.; Toyota, K.; Fukuda, R.; Hasegawa, J.; Ishida, M.; Nakajima, T.; Honda, Y.; Kitao, O.; Nakai, H.; Vreven, T.; Montgomery, Jr., J. A.; Peralta, J. E.; Ogliaro, F.; Bearpark, M.; Heyd, J. J.; Brothers, E.; Kudin, K. N.; Staroverov, V. N.; Kobayashi, R.; Normand, J.; Raghavachari, K.; Rendell, A.; Burant, J. C.; Iyengar, S. S.; Tomasi, J.; Cossi, M.; Rega, N.; Millam, J. M.; Klene, M.; Knox, J. E.; Cross, J. B.; Bakken, V.; Adamo, C.; Jaramillo, J.; Gomperts, R.; Stratmann, R. E.; Yazyev, O.; Austin, A. J.; Cammi, R.; Pomelli, C.; Ochterski, J. W.; Martin, R. L.; Morokuma, K.; Zakrzewski, V. G.; Voth, G. A.; Salvador, P.; Dannenberg, J. J.; Dapprich, S.; Daniels, A. D.; Farkas, Ö.; Foresman, J. B.; Ortiz, J. V.; Cioslowski, J.; Fox, D. J. *Gaussian 03*, revision C.01; Gaussian, Inc.: Wallingford CT, 2004.
23. TURBOMOLE (version 5.6); Universität Karlsruhe, 2000.

24. Jacquemin, D.; Perpète, E. A.; Ciofini, I.; Adamo, Valero, R.; Zhao, Y; Truhlar, D.G. *J. Chem. Theory Comput.* **2010**, *6*, 2071–2085.
25. Mathew, S.; Yella, A.; Gao, P.; Humphry-Baker, R.; Curchod, F.E.; Ashari-Astani, N.; Tavernelli, I.; Rothlisberger, U.; Nazeeruddin, M. K.; Grätzel, M. *Nature Chem.* **2014**, *6*, 242–247.
26. (a) J. Peet, J. Y. Kim, N. E. Coates, W. L. Ma, D. Moses, A. J. Heeger and G. C. Bazan, *Nat. Mater.*, 2007, *6*, 497; (b) M. S. Su, C. Y. Kuo, M. C. Yuan, U. S. Jeng, C. J. Su and K. H. Wei, *Adv. Mater.*, 2011, *23*, 3315;
27. He, Y. J.; Chen, H. Y.; Hou, J. H.; Li, Y. F. *J. Am. Chem. Soc.* 2010, *132*, 1377–1382.
28. Blom, P. W. M.; de Jong, M.J.M.; Munster, M.G.van *Phys. Rev. B: Condens. Matter Mater. Phys.*, **1997**, *55*, R656.
29. Honggi Kim, Hyungjin Lee, Donghyun Seo, Youngjun Jeong, Keun Cho, Jaechol Lee, Youngu Lee, *Chem. Mater.* doi: 10.1021/acs.chemmater.5b00632
30. (a) Wang, M.; Wang, H.; Yokoyama, T.; Liu, X.; Huang, Y.; Zhang, Y.; Nguyen, T. Q.; Aramaki, S.; Bazan, G. C. *J. Am. Chem. Soc.*, **2014**, *136*, 12576, (b) Deng, Y.; Liu, J.; Wang, J.; Liu, L.; Li, W.; Tian, H.; Zhang, X.; Xie, Z.; Geng, Y.; Wang, F.; *Adv. Mater.*, **2014**, *26*, 471.
31. Lou, S. J.; Szarko, J. M.; Xu, T.; Yu, L.; Marks, T. J.; Chen, L. X. *J. Am. Chem. Soc.*, **2011**, *133*, 20661.
32. Z. Mao, T. P. Le, K. Vakhshouri, R. Fernando, F. Ruan, E. Muller, E. D. Gomez and G. Sauve', *Org. Electron.* **2014**, *15*, 3384–3391.
33. (a) R. A. Street, A. Krakaris and S. R. Cowan, *Adv. Funct. Mater.* 2012, *22*, 4608, (b) Z. He, C. Zhong, X. Huang, W.-Y. Wong, H. Wu, L. Chen, S. Su and Y. Cao, *Adv. Mater.*, 2011, *23*, 4636

Table 1 Photophysical and electrochemical properties of **P1** and **P2** in solution and the thin films.

Copolymer	$\lambda_{\max}^{\text{solution}}$ (nm)	$\lambda_{\max}^{\text{film}}$ (nm)	$\lambda_{\text{onset}}^{\text{film}}$ (nm)	$E_g^{\text{opt}}$ (eV)	$E_{\text{HOMO}}$ (eV)	$E_{\text{LUMO}}$ (eV)	$E_g^{\text{ec}}$ (eV)
<b>P1</b>	282,568	284,592	707	1.75	5.40	3.40	2.00
<b>P2</b>	280,553	281,578	693	1.79	5.31	3.33	1.96

Table 2 Calculated properties of **P1** and **P2**. Specifically, HOMO and LUMO energies (eV), HOMO–LUMO gap (eV), *HL*, Optical gap (eV), *OG*, with corresponding oscillator strengths, *f*, the wavelengths of the first excitation and excitations with the largest oscillator strengths, the main contributions to the first excited state, and the dipole moment ( $\mu$ ).

	HOM O (eV)	LUMO (eV)	HL (eV)	OG (eV)	$\lambda_{1\text{st}/\text{max}}$ (nm)	<i>f</i>	Main Contributions	$\mu$ (D)
<b>P1</b>								
<b>PBE</b>	-4.28	-2.95	1.33	1.74	714	1.15	H→L (81%), H→L+1 (13%), H-1->L (6%)	2.49
	-4.41 <sup>a</sup>	-3.07 <sup>a</sup>	1.34 <sup>a</sup>	1.66 <sup>a</sup>	747 <sup>a</sup>	1.61 <sup>a</sup>	H→L (93%), H→L+1 (5%) <sup>a</sup>	2.75 <sup>a</sup>
<b>B3LY P</b>	-4.84	-2.49	2.36	2.14	579/435/376/291	1.86	H→L (99%)	2.34
	-4.95 <sup>a</sup>	-2.59 <sup>a</sup>	2.36 <sup>a</sup>	2.05 <sup>a</sup>	604/447/376/298/290 <sup>a</sup>	2.09 <sup>a</sup>	H→L (99%) <sup>a</sup>	2.37 <sup>a</sup>
<b>M06</b>	-5.17	-2.41	2.75	2.24	554/420/353/279	1.85	H→L (97%)	2.18
	-5.29 <sup>a</sup>	-2.53 <sup>a</sup>	2.76 <sup>a</sup>	2.15 <sup>a</sup>	576/436/353/289/279 <sup>a</sup>	2.06 <sup>a</sup>	H→L (96%) <sup>a</sup>	2.20 <sup>a</sup>
<b>P2</b>								
<b>PBE</b>	-4.27	-2.93	1.34	1.79	693	1.65	H→L (98%)	4.35
	-4.40 <sup>a</sup>	-3.05 <sup>a</sup>	1.35 <sup>a</sup>	1.69 <sup>a</sup>	734 <sup>a</sup>	1.86 <sup>a</sup>	H→L (98%) <sup>a</sup>	5.42 <sup>a</sup>
<b>B3LY P</b>	-4.83	-2.46	2.37	2.15	576/429/371/292	1.89	H→L (99%)	4.47
	-4.95 <sup>a</sup>	-2.57 <sup>a</sup>	2.37 <sup>a</sup>	2.06 <sup>a</sup>	602/444/375/307/291 <sup>a</sup>	2.12 <sup>a</sup>	H→L (99%) <sup>a</sup>	5.29 <sup>a</sup>
<b>M06</b>	-5.15	-2.38	2.77	2.24	552/414/349/295/281	1.86	H→L (97%)	4.50
	-5.28 <sup>a</sup>	-2.50 <sup>a</sup>	2.78 <sup>a</sup>	2.16 <sup>a</sup>	574/441/351/295/279 <sup>a</sup>	2.07 <sup>a</sup>	H→L (97%) <sup>a</sup>	5.28 <sup>a</sup>

<sup>a</sup> Values when solvent effects are taken into account for chloroform.

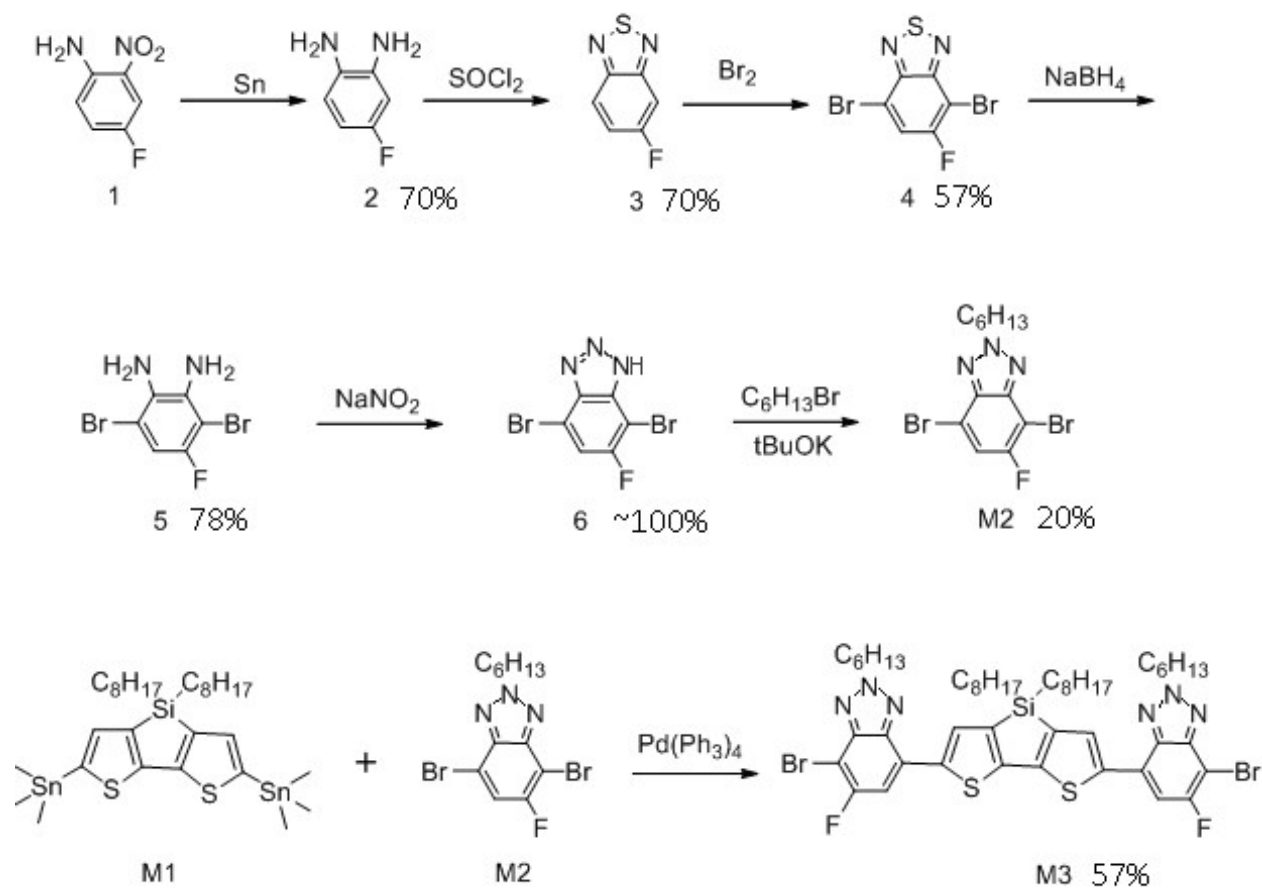
Table 3 Photovoltaic parameters of PSCs based on **P1**:PC<sub>71</sub>BM (1:2) and **P2**:PC<sub>71</sub>BM (1:2) processed with CF and DIO (3v%)/CF solvents

Active layers	J <sub>sc</sub> (mA/cm <sup>2</sup> )	V <sub>oc</sub> (V)	FF	PCE (%)	R <sub>s</sub> (Ωcm <sup>2</sup> )	R <sub>sh</sub> (Ωcm <sup>2</sup> )
<b>P1</b> :PC <sub>71</sub> BM (1:2) <sup>a</sup>	8.58	0.98	0.46	3.87 (3.78) <sup>c</sup>	28.12	376
<b>P2</b> :PC <sub>71</sub> BM (1:2) <sup>a</sup>	6.88	0.92	0.42	2.53 (2.45) <sup>c</sup>	26.24	413
<b>P1</b> :PC <sub>71</sub> BM (1:2) <sup>b</sup>	12.82	0.92	0.65	7.66 (7.54) <sup>c</sup>	14.56	456
<b>P2</b> :PC <sub>71</sub> BM (1:2) <sup>b</sup>	10.64	0.88	0.56	5.33 (5.32) <sup>c</sup>	22.24	389

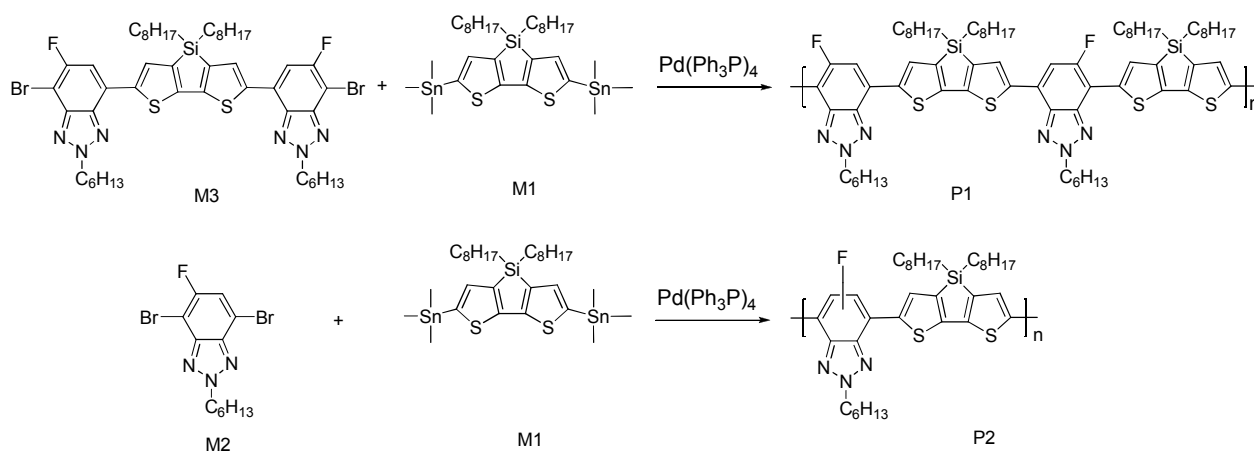
<sup>a</sup>As cast from CF

<sup>b</sup>DIO (3v%)/CF cast

<sup>c</sup>average of 5 devices



Scheme 1 Synthetic routes toward M3



Scheme 2. Synthetic route polymers P1 and P2

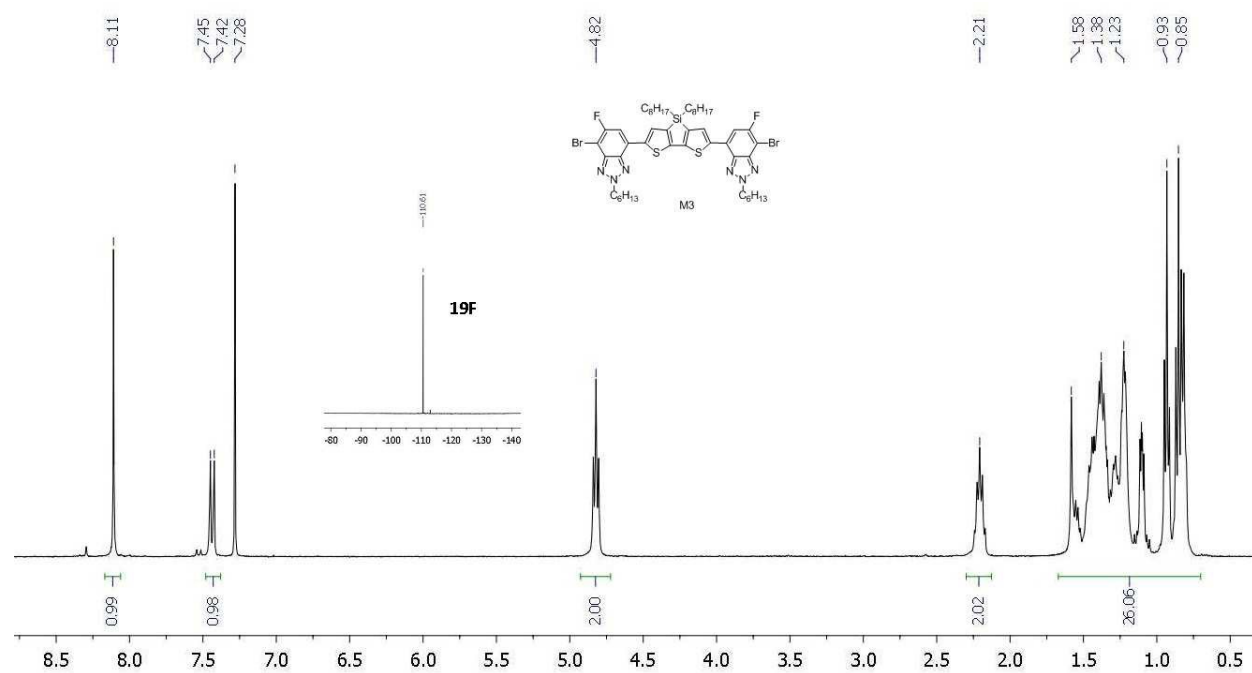
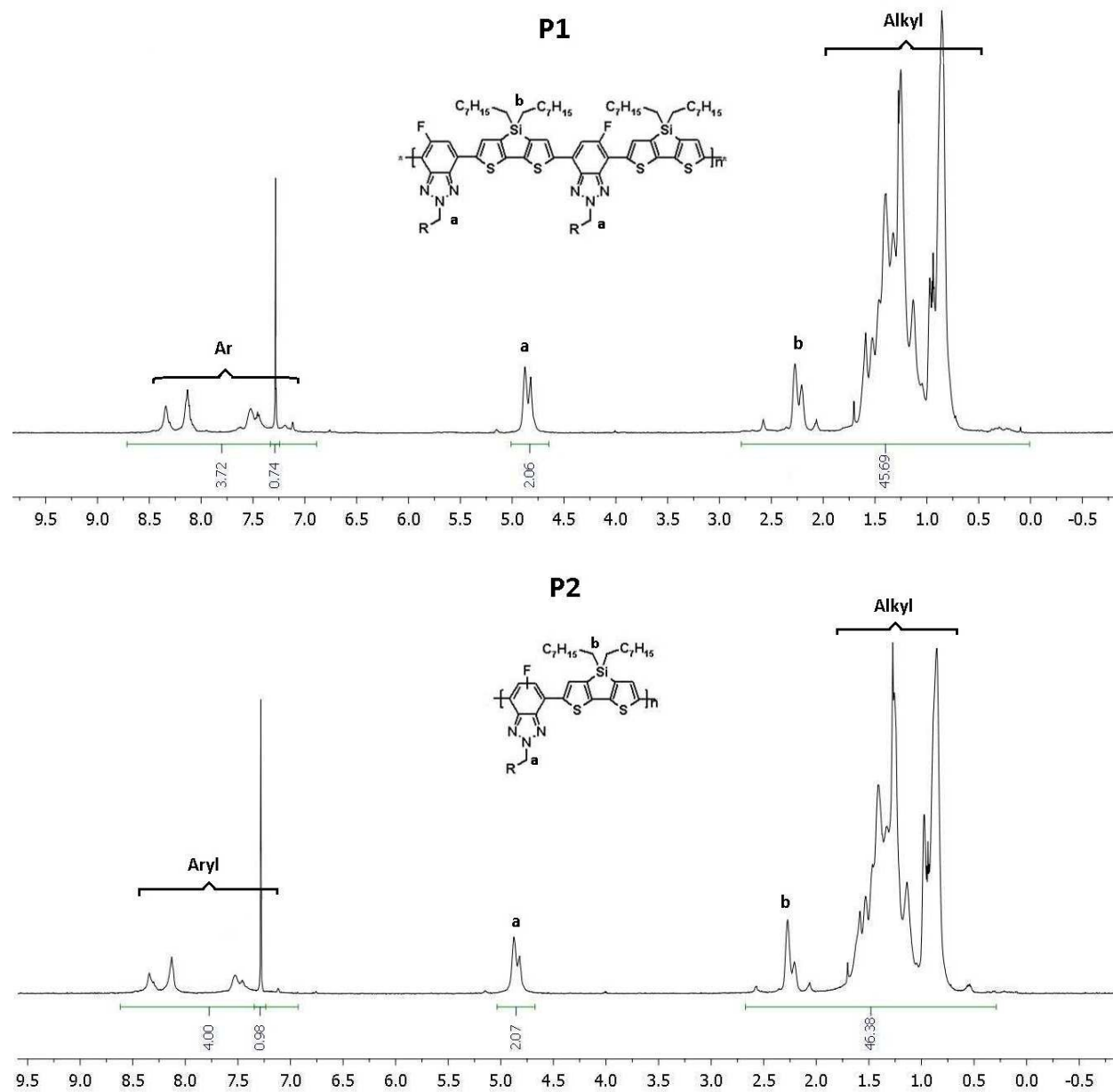


Figure 1  $^1\text{H}$  and  $^{19}\text{F}$  NMR of 2,6-bis(7-bromo-6-fluoro-2-hexyl-2*H*-benzotriazol-4-yl)-4,4-bis(2-ethylhexyl)-4*H*-silolo[3,2-*b*:4,5-*b'*]dithiophene (**M3**)

Figure 2 <sup>1</sup>H NMR spectra of polymers P1 and P2

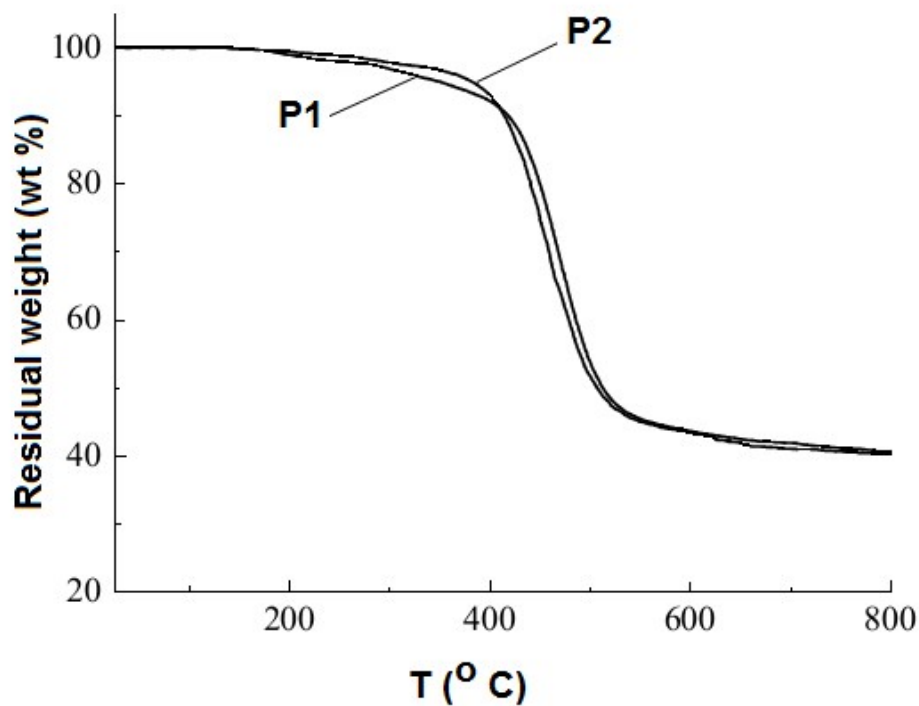


Figure 3 TGA curves of polymers **P1** and **P2** at a heating rate of  $10^{\circ}\text{C min}^{-1}$

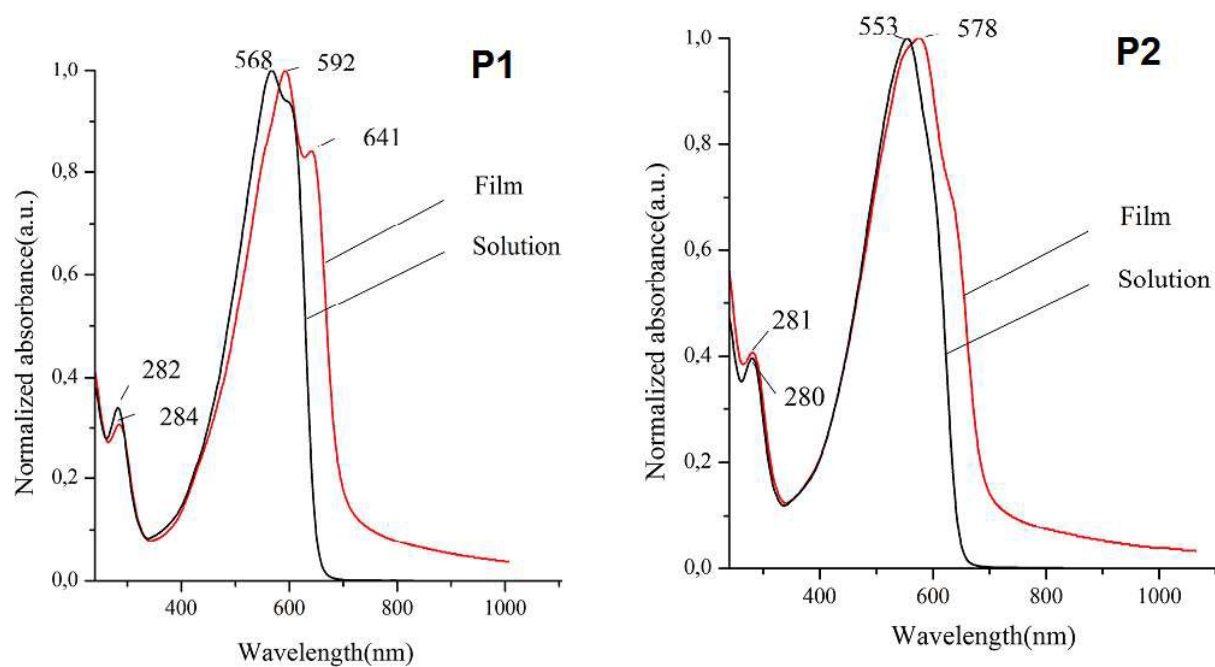


Figure 4 Normalized UV-vis absorption spectra of **P1** and **P1** in chloroform dilute solution (black color) and in the solid state (red color)

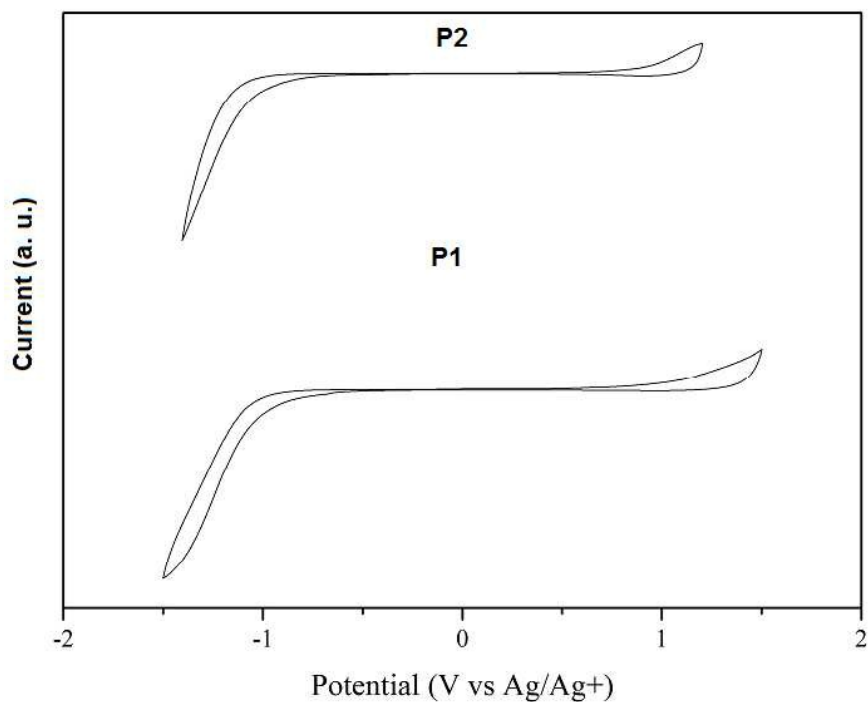


Figure 5 Cyclic voltammograms of **P1** and **P2** in a acetonitrile solution of 0.1M  $\text{Bu}_4\text{NPF}_6$  with a scan rate of  $100\text{mVs}^{-1}$

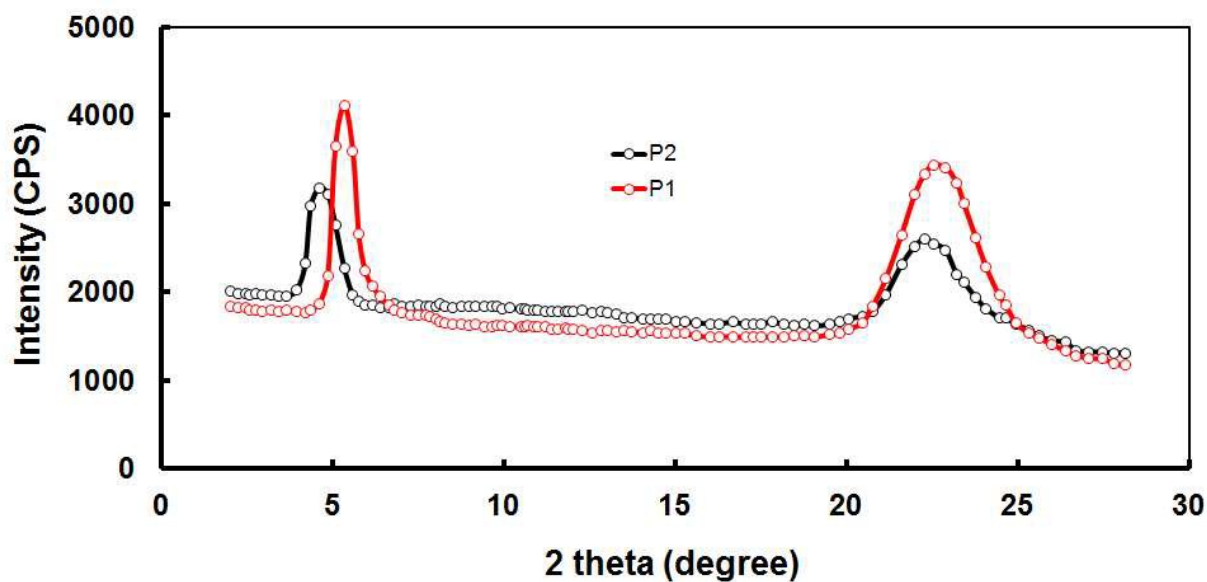


Figure 6 XRD patterns of P1 and P2 thin films

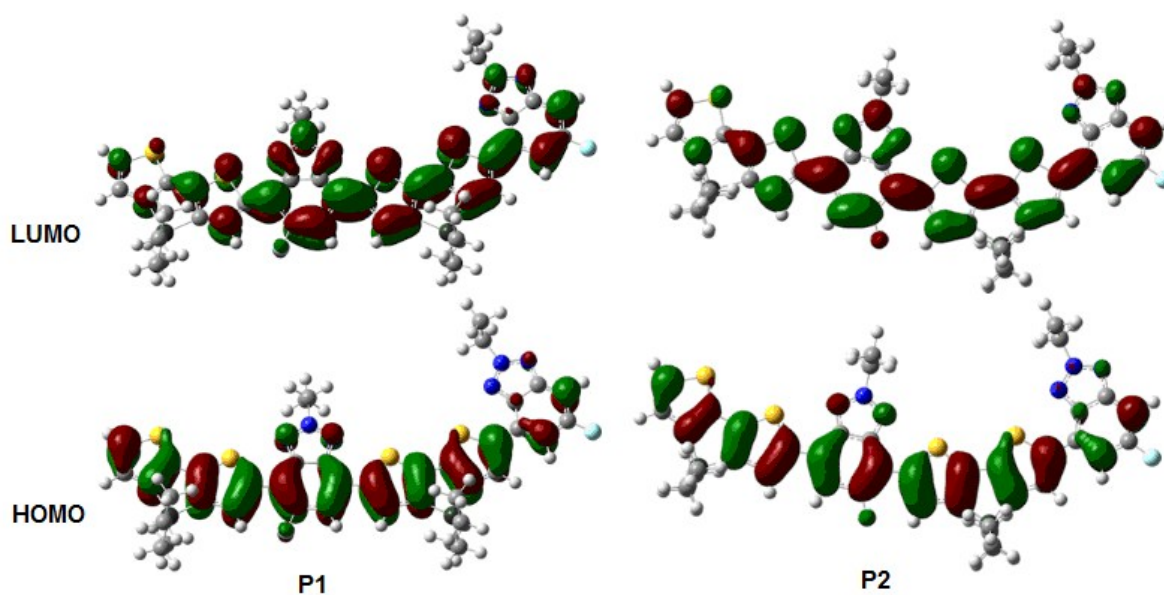


Figure 7 Frontier orbitals of (left) **P1** and (right) **P2**

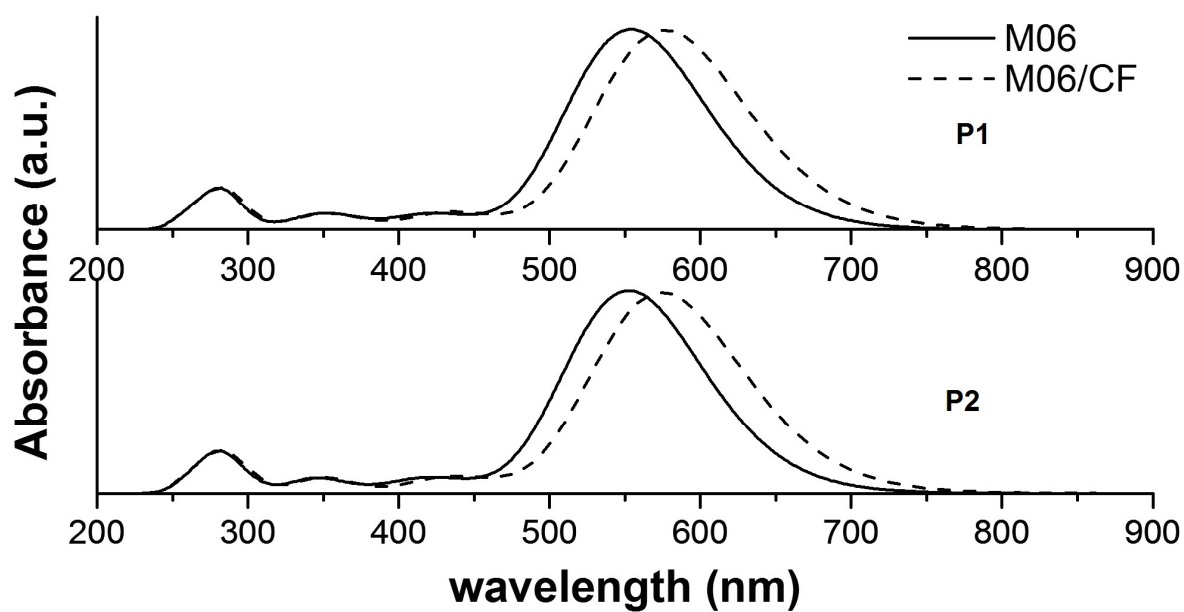


Figure 8 Theoretical UV/Vis absorption spectrum of (top) **P1** and (bottom) **P2** (calculated using the M06 functional).

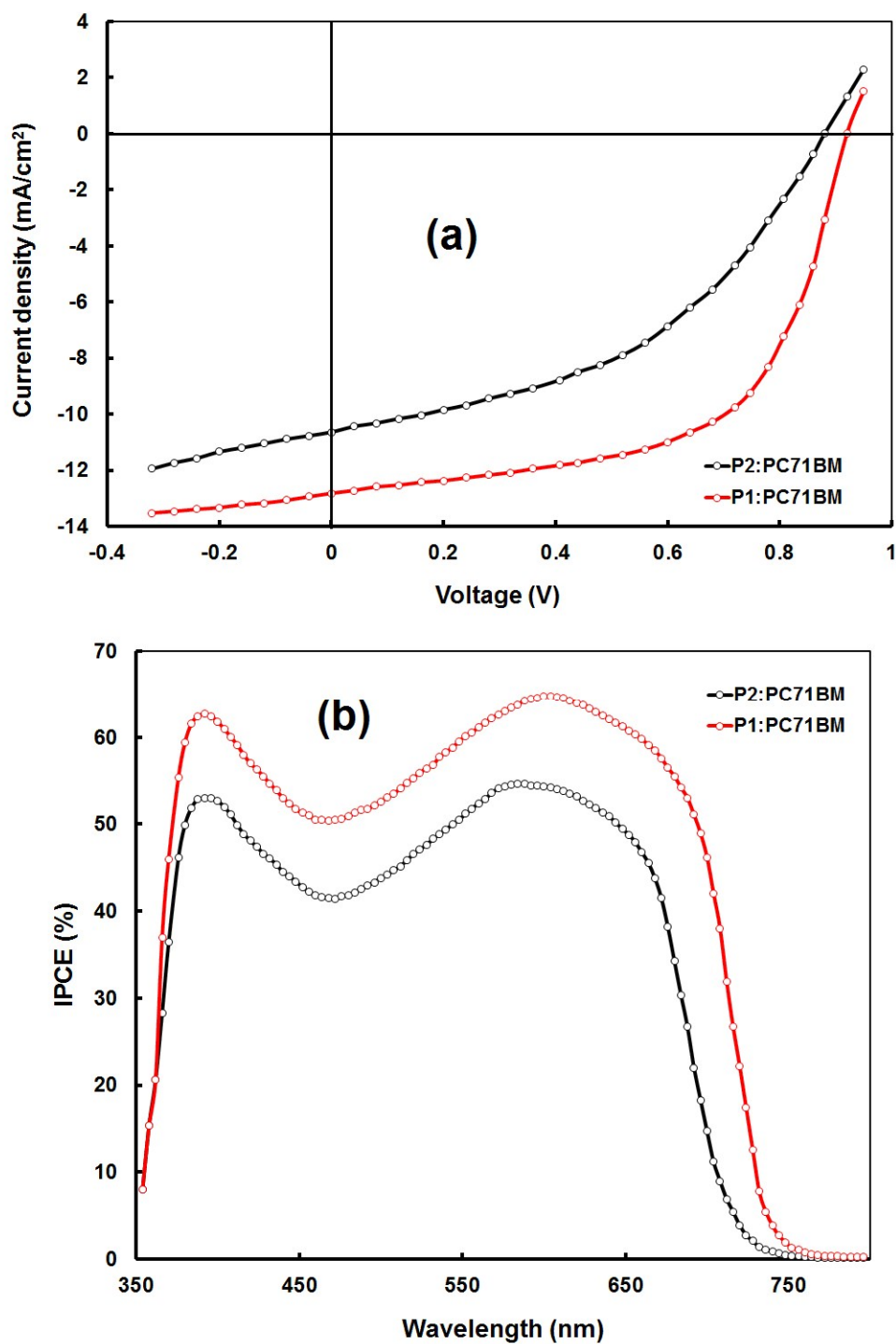


Figure 9 (a) J-V characteristics under illumination and (b) IPCE spectra of the PSCs based on P1:PC<sub>71</sub>BM (1:2) and P2:PC<sub>71</sub>BM (1:2) cast from DIO (3v%)/CF

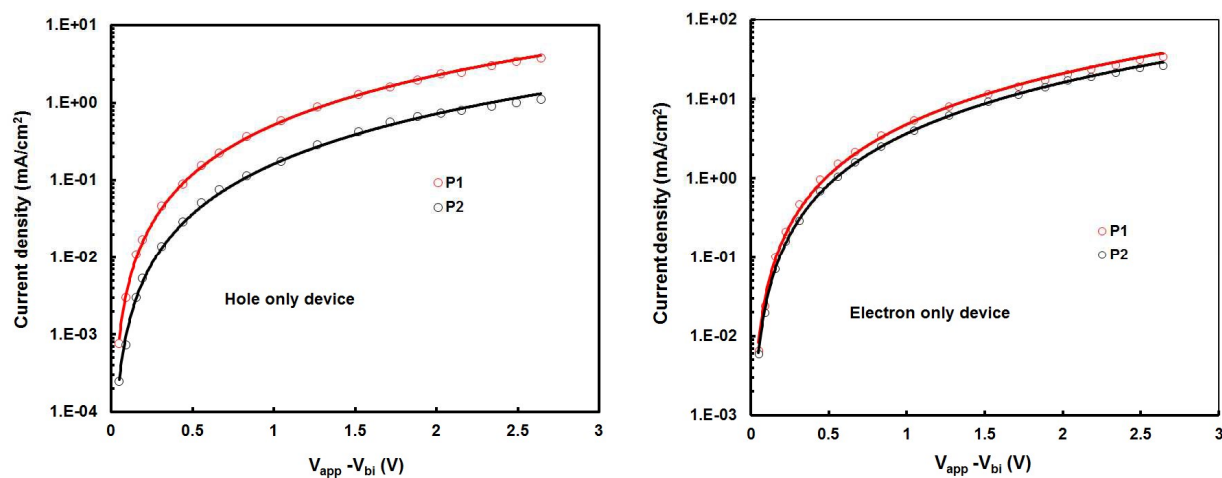


Figure 10 J-V characteristics in dark of hole and electron only devices

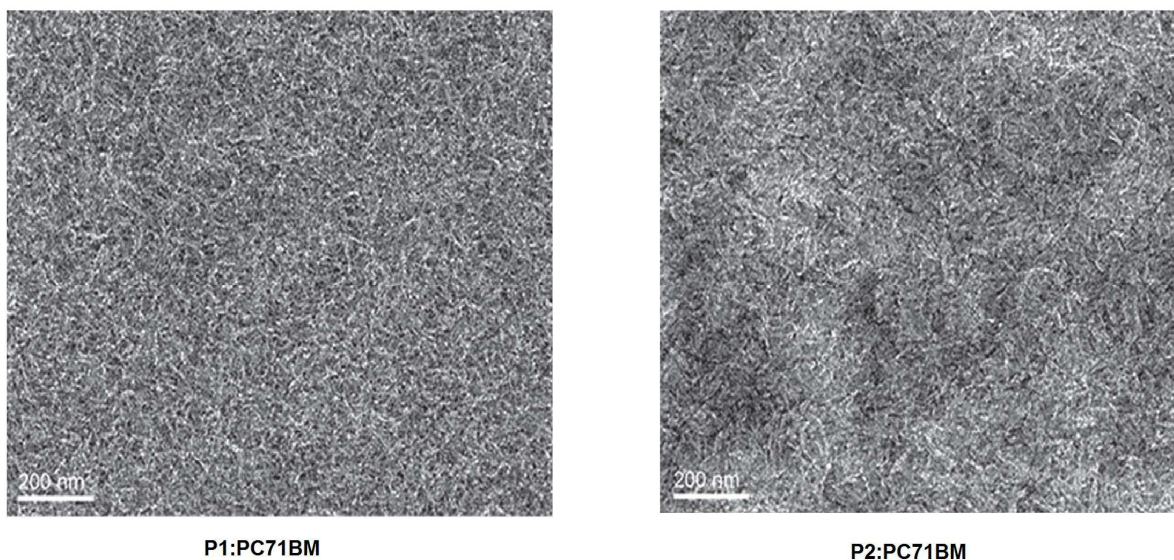


Figure 11 TEM images of **P1**:PC<sub>71</sub>BM and **P2**:PC<sub>71</sub>BM cast from DIO/CF solution

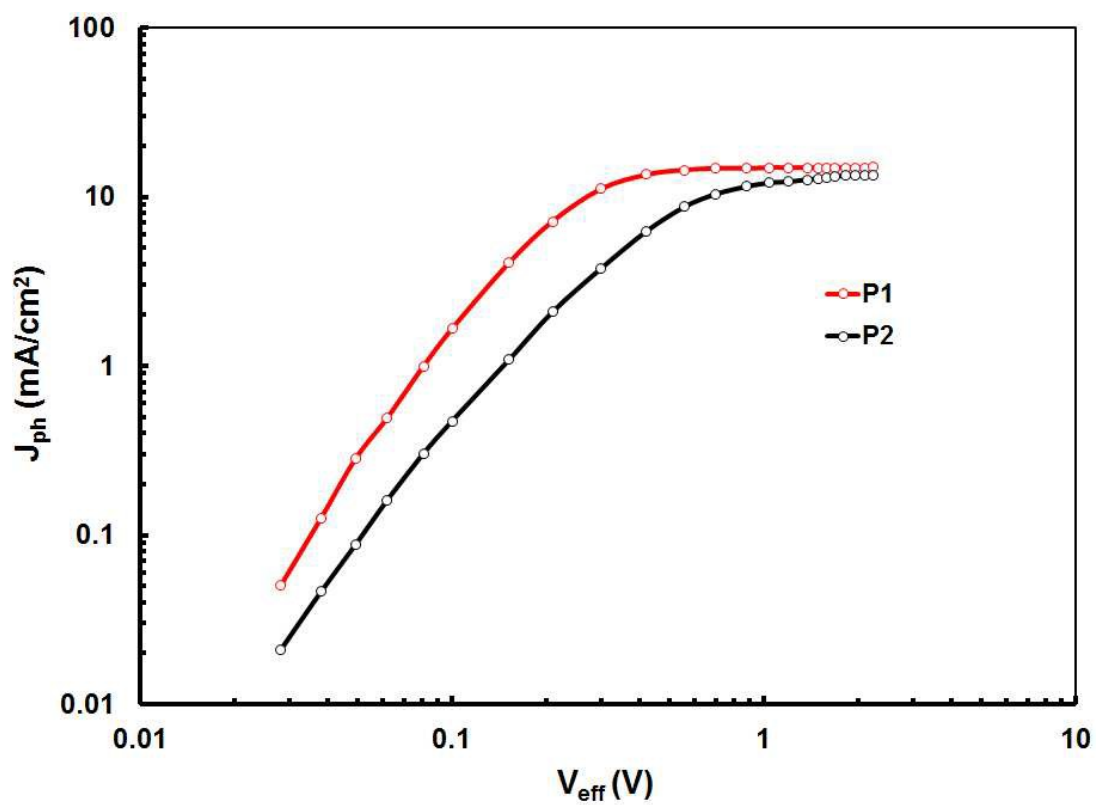


Figure 12 Photocurrent density ( $J_{ph}$ ) variation with effective voltage ( $V_{eff}$ ) for the PSC with **P1**:PC71BM and **P2**:PC<sub>71</sub>BM

## TOC

